

# Storage density of shift-multiplexed holographic memory

Gregory J. Steckman, Allen Pu, and Demetri Psaltis

The storage density of shift-multiplexed holographic memory is calculated and compared with experimentally achieved densities by use of photorefractive and write-once materials. We consider holographic selectivity as well as the recording material's dynamic range ( $M/\#$ ) and required diffraction efficiencies in formulating the calculations of storage densities, thereby taking into account all major factors limiting the raw storage density achievable with shift-multiplexed holographic storage systems. We show that the  $M/\#$  is the key factor in limiting storage densities rather than the recording material's thickness for organic materials in which the scatter is relatively high. A storage density of 100 bits/ $\mu\text{m}^2$  is experimentally demonstrated by use of a 1-mm-thick  $\text{LiNbO}_3$  crystal as the recording medium.

© 2001 Optical Society of America

OCIS codes: 090.7330, 090.4220, 210.2860.

## 1. Introduction

One of the most important attributes of holographic data storage is its potential for high storage densities.<sup>1</sup> In practice, the achievable density is limited by the quality of the holographic recording material. A holographic material should have sufficient thickness for low cross talk, high dynamic range for a large recovered signal strength, long-term hologram stability, and nondestructive readout. Recent progress in materials research in photorefractives<sup>2-4</sup> and write-once photopolymers<sup>5-7</sup> shows promise for addressing the material issues.

Our purpose in this paper is to address specifically the influences of material thickness and the material's dynamic range ( $M/\#$ ) on the storage density achievable with shift-multiplexed holographic disk systems.<sup>8</sup> Past analyses on the storage capacity of holographic storage systems<sup>8-10</sup> have considered only the influence of geometric constraints, such as material thickness on storage densities, without taking into account the limits imposed by the  $M/\#$ . When both geometric and dynamic range factors are included, a more accurate

prediction of potential storage densities can be made. Furthermore, these predictions can act as a guide for material researchers who need to obtain a minimum level of performance before their materials are ready to be implemented in high-density holographic storage systems.

In Section 2 a description of the optical system considered is described followed by the calculations necessary to compute the holographic data-storage density of such a system. Variations of the calculation for use with rewritable photorefractive or write-once photopolymer materials are presented. Because the derived formulas are, in general, transcendental, and optimizations over many parameters are required, numerical techniques are used to solve the calculation problem, specifically a genetic algorithm. In Section 3 calculated values for storage density are compared with experimentally obtained densities from shift-multiplexing experiments with both lithium niobate and a write-once photopolymer. Finally, calculations of possible data-storage densities with shift-multiplexed holographic memories are made relative to the performance and thickness of the storage material and the wavelength of light used.

## 2. Calculation of Storage Density

A typical configuration for a shift-multiplexed holographic storage system is shown in Fig. 1. Lenses L1 and L2 form a 4- $f$  imaging system between the data signal imprinted onto the signal beam and a CCD detector used to detect the reconstructed holograms. The recording material is placed near the Fourier plane of the signal. A spherical reference beam is created with lens L3, positioned such that the reference beam completely

---

When this research was performed the authors were with the Department of Electrical Engineering, California Institute of Technology, Mail Stop 136-93, Pasadena, California 91125. G. J. Steckman (e-mail: steckman@sunoptics.caltech.edu) is now with Ondax, Inc., 850 East Duarte Road, Monrovia, California 91016. A. Pu is now attending The Anderson School, University of California, Los Angeles, Los Angeles, California 90095-1481 for his master of business administration.

Received 26 April 2000; revised manuscript received 20 March 2001.

0003-6935/01/203387-08\$15.00/0

© 2001 Optical Society of America

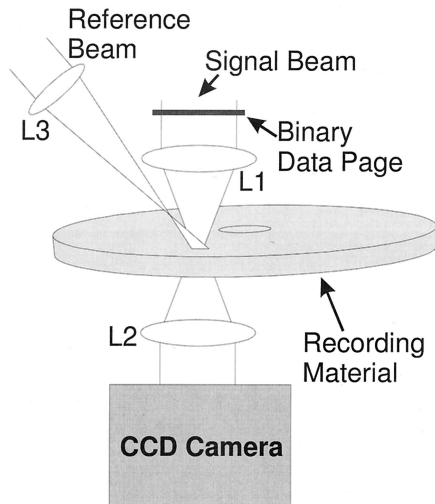


Fig. 1. Typical configuration for a shift-multiplexed holographic storage system.

overlaps the signal beam throughout the material. Rotation of the disk serves as the in-plane shift mechanism, and radial translations of the optical system access different tracks.

The storage density for a holographic disk system that uses shift multiplexing can be computed by the relation  $D = N_p / (\delta \times \delta_r)$ , where  $N_p$  is the number of bits stored per hologram.  $\delta$  is the shift distance required between holograms to reconstruct them without substantial cross talk and to limit the number of overlapped holograms to obtain sufficient diffraction efficiency.  $\delta_r$  is the radial shift distance required between tracks of holograms.  $N_p$  and  $\delta_r$  are determined by the optical system and material thickness, whereas  $\delta$  is determined from shift selectivity and dynamic range limitations.

A requirement of the optical system is to have the reference beam completely overlap the signal beam throughout the volume of the material. Each beam will form an ellipse on the top and bottom surfaces of the material. The sizes and positions of the four ellipses are first determined in Subsections 2.A and 2.B. The beam ellipses are used for two purposes. First, by comparing the sizes and positions of the ellipses we can ensure that the signal and reference beams will completely overlap each other on both the first and second surfaces of the recording material. If complete overlapping is not obtained, the density is computed as zero. Second, the sizes of the beams are needed to determine the shift distances required between adjacent holograms when we take into account the M/#.

#### A. Reference Beam Geometry

Geometrical optics is used to determine the area of the recording material that is illuminated by the reference beam. In Fig. 2 the reference beam is completely specified by the position of its focus  $x_f$  and  $z_f$ , the divergence angle  $\phi$ , and its angle relative to the material's surface normal  $\theta$ .  $z_f$  is the distance of the reference beam focus from the material along a line

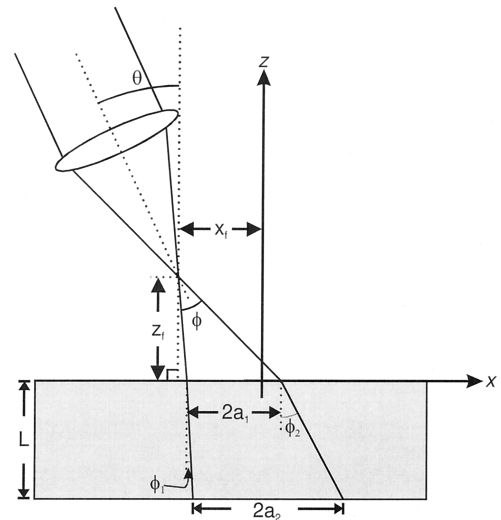


Fig. 2. Reference beam geometry used to compute the area occupied on a recording material's surface.

normal to the material's surface.  $x_f$  is defined relative to the intersection of the signal beam with the first surface of the material, as defined by the origin of the coordinate system shown in Fig. 4.  $L$  is the thickness of the recording material, and  $n$  is its index of refraction. The beam forms an ellipse on the top and bottom surfaces of the material, given by

$$\frac{(x - x_i)^2}{a_i^2} + \frac{y^2}{b_i^2} = 1, \quad (1)$$

where index  $i$  is 1 for the surface closer to the focus and 2 is for the surface further from the focus.

For the top surface of the material, the reference beam can be specified with the parameters calculated as

$$\begin{aligned} a_1^r &= \frac{z_f}{2} [\tan(\theta + \phi/2) - \tan(\theta - \phi/2)], \\ b_1^r &= z_f \frac{\tan(\phi/2)}{\cos(\theta)}, \\ x_1^r &= x_f + a_1^r + z_r \tan(\theta - \phi/2), \end{aligned} \quad (2)$$

which is a straightforward application of trigonometry to the angles of the beam and its divergence together with its position. The reference beam is tilted only in the plane of the signal and the normal to the surface. Before we write the formula for the parameters of the ellipse on the second surface, it is convenient to first introduce the notation for the beam angles inside the material. The divergence of the reference beam inside the material can be divided into two angles, one corresponding to each edge of the beam. Each edge is refracted according to Snell's law:

$$\begin{aligned} \phi_1 &= \arcsin \left[ \frac{\sin(\theta - \phi/2)}{n} \right], \\ \phi_2 &= \arcsin \left[ \frac{\sin(\theta + \phi/2)}{n} \right]. \end{aligned} \quad (3)$$

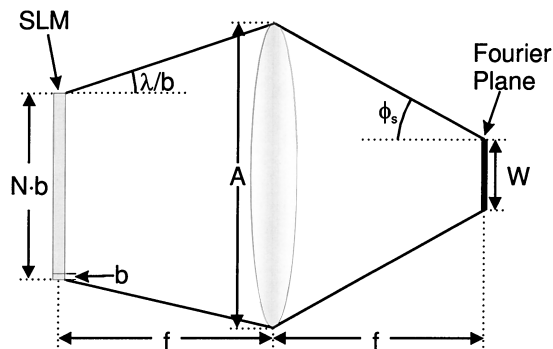


Fig. 3. Diffraction from a SLM forming the Fourier plane of the signal beam.

The parameters of the ellipse on the surface further from the focal point are now easily written in terms of the parameters on the first surface as

$$\begin{aligned} a_2^r &= a_1^r + \frac{L}{2} [\tan(\phi_2) + \tan(\phi_1)], \\ b_2^r &= b_1^r + L \tan\left\{\arcsin\left[\frac{\sin(\phi/2)}{n}\right]\right\}, \\ x_2^r &= x_1^r + \frac{L}{2} [\tan(\phi_1) + \tan(\phi_2)]. \end{aligned} \quad (4)$$

#### B. Signal Beam Geometry

In the system under consideration the signal beam is modulated with a spatial light modulator (SLM) and focused with a lens. The recording material is placed just after the Fourier plane of the incident signal. In Fig. 3, under the paraxial approximation, the properties of a focused signal beam can be computed on the basis of the pixel size used,  $b$ , the number of pixels across the SLM,  $N$ , the diameter of the lens being used,  $A$ , and the focal length of the lens,  $f$ . However, not all these parameters are independent. From Fig. 3 it is easy to see that there is a relationship between the lens' focal length and aperture size relative to the number of pixels used and the size of each pixel. The incident beam is diffracted at an angle given by  $\lambda/b$ , allowing  $N$  to be computed, given a fixed  $A$  and  $f$ , as

$$N = \frac{A}{b} - \frac{2\lambda f}{b^2}. \quad (5)$$

If more pixels than this are used, the light diffracted from those pixels at the edge of the SLM will not be sufficiently collected by the lens, and ultimately distortion will occur in the imaging system.  $Nb$  is therefore the effective diameter of a circle of pixels that will be adequately imaged by the optical system. The total number of square

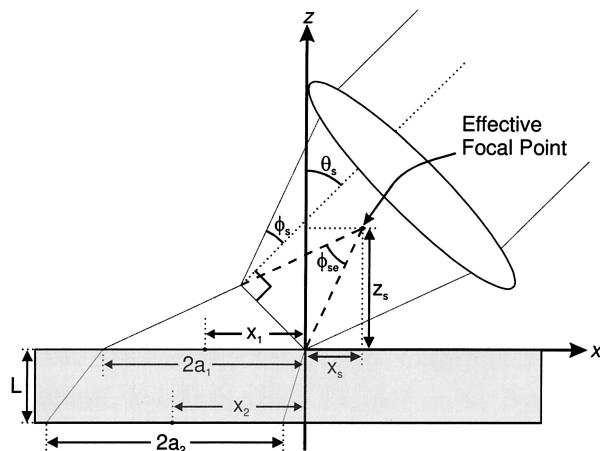


Fig. 4. Geometry of the signal beam to compute the area covered on a recording material's surface.

pixels with an edge of length  $b$  fitting in this circle is given by

$$N_p = \frac{\pi \left(\frac{Nb}{2}\right)^2}{b^2} = \frac{\pi}{4} N^2. \quad (6)$$

After the lens, the signal forms a converging beam with an angle given by

$$\phi_s = \frac{Nb}{2f}. \quad (7)$$

The size of the Fourier plane, when we consider only the fundamental order, is given by

$$W = \frac{2\lambda f}{b}. \quad (8)$$

To compute the area of the recording material illuminated by the signal beam, the signal beam tilt angle  $\theta_s$  must also be accounted for. For the derivation of the ellipse parameters for the areas illuminated on the two surfaces of the disk by the signal beam, we can use the technique developed for the reference beam by realizing that the diverging signal beam after the Fourier plane can be converted into an effective point source, as shown in Fig. 4. Although the signal beam is not a spherical wave as in the case for the reference beam, the approach is geometrically applicable. The parameters of the equivalent point source can be computed in terms of the other signal beam properties as

$$\begin{aligned} \phi_{se} &= \frac{Nb}{f}, \\ x_s &= \frac{\lambda f \sin(\theta_s - \phi_{se}/2)}{b \sin(\phi_{se}/2)}, \\ z_s &= \frac{\lambda f \cos(\theta_s - \phi_{se}/2)}{b \sin(\phi_{se}/2)}. \end{aligned} \quad (9)$$

Similarly to the case with the reference beam, the parameters of the signal beam ellipse for the first surface are readily calculated as

$$\begin{aligned} a_1^s &= \frac{z_s}{2} [\tan(\theta_s + \phi_{se}/2) - \tan(\theta_s - \phi_{se}/2)], \\ b_1^s &= z_s \frac{\tan(\phi_{se}/2)}{\cos(\theta_s)}, \\ x_1^s &= x_s - a_1^s - z_s \tan(\theta_s - \phi_{se}/2). \end{aligned} \quad (10)$$

The internal angles of the diverging signal beam are then

$$\begin{aligned} \phi_1^s &= \arcsin \left[ \frac{\sin(\theta_s - \phi_{se}/2)}{n} \right], \\ \phi_2^s &= \arcsin \left[ \frac{\sin(\theta_s + \phi_{se}/2)}{n} \right]. \end{aligned} \quad (11)$$

Written in terms of the ellipse parameters for the first surface, the ellipse of the signal beam on the second surface of the material is given by the parameters

$$\begin{aligned} a_2^s &= a_1^s + \frac{L}{2} [\tan(\phi_2^s) + \tan(\phi_1^s)], \\ b_2^s &= b_1^s + L \tan \left\{ \arcsin \left[ \frac{\sin(\phi_{se}/2)}{n} \right] \right\}, \\ x_2^s &= x_1^s + \frac{L}{2} [\tan(\phi_1^s) + \tan(\phi_2^s)]. \end{aligned} \quad (12)$$

### C. Density for Read-Only and Rewritable Materials

For write-once materials, the width of each hologram in the along-track direction is given by the size of the reference beam:

$$W_{ip} = 2a_2^r. \quad (13)$$

For rewritable materials, the portion of the reference beam incident on unrecorded material does not need to be counted. Therefore the shift distance that would be required to record two completely nonoverlapping holograms is less than the total length of the exposed area on the material during recording. This distance can be different depending on the shift direction, but should be taken as the minimum because it will allow higher storage densities. The along-track shift distance can be computed from

$$\begin{aligned} W_{ip} &= \min[|x_2^r + a_2^r - (x_2^s - a_2^s)|, \\ &|x_2^r - a_2^r - (x_2^s + a_2^s)|]. \end{aligned} \quad (14)$$

For the beam width in the radial direction, that portion of the reference beam that would not overlap the signal beam can be blocked with an aperture. In this case the effective width is the same as that of the signal beam:

$$W_{op} = 2b_2^s. \quad (15)$$

The shift distance between adjacent holograms is determined when we take the maximum of two dif-

ferent constraints, the shift selectivity and the dynamic range limitation. According to Ref. 8, after we take into account the tilt of the reference beam, the shift required between adjacent holograms to satisfy the selectivity constraint is

$$\delta_s = P \left[ \frac{\lambda \cos(\theta_{si}) \left( z_f + \frac{L}{2n} \right)}{L \cos^2(\theta_{ri}) \sin(\theta_{si} + \theta_{ri})} + \frac{\lambda}{2 \sin(\phi_r/2)} \right], \quad (16)$$

where  $P$  is a number greater than 1 used to indicate the number of null distances to shift between holograms. If  $P$  is increased, it will reduce noise associated with cross talk, but will decrease the storage density. It is assumed here that  $P$  is chosen such that cross-talk noise can be ignored compared with other noise sources, predominantly scatter noise.  $\theta_{si}$  and  $\theta_{ri}$  are the center angles of the signal and reference beams, respectively, after they are corrected for refraction. Equation (16) must be modified slightly because, for the situation being considered, the signal beam is not a plane wave but rather has a bandwidth. The shift selectivity will therefore become worse because some components of the signal beam have angles that are less than  $\theta_{si}$ . If the shift distance is not large enough to satisfy the selectivity constraint for all signal beam angles, cross talk will result at one edge of the reconstructed signal beam because angles at the Fourier plane correspond to spatial position in the image plane. To avoid using a shift distance that is too small, one should use the minimum internal signal beam angle, yielding for the shift selectivity the formula

$$\delta_s = P \left[ \frac{\lambda \cos(\phi_1^s) \left( z_f + \frac{L}{2n} \right)}{L \cos^2(\theta_{ri}) \sin(\phi_1^s + \theta_{ri})} + \frac{\lambda}{2 \sin(\phi_r/2)} \right]. \quad (17)$$

With a suitable choice for  $P$ , Eq. (17) will ensure that cross-talk noise is not a problem. However, the shift selectivity does not take into account the limitation of the  $M/\#$ . The relationship between the  $M/\#$  and the diffraction efficiency of  $M$  stored holograms is given by<sup>11</sup>

$$\eta = \left( \frac{M/\#}{M} \right)^2, \quad (18)$$

where the diffraction efficiency is assumed to be equal for each of the stored holograms. To have a sufficient signal-to-noise ratio (SNR) of the reconstructed holograms, a minimum diffraction efficiency must be achieved. Therefore, by fixing the diffraction efficiency required, we can compute the absolute maximum number of holograms that can overlap. Given the maximum allowable  $M$ , the shift distance between holograms required to avoid overlapping too many holograms at the same location is given by

$$\delta_M = \frac{W_{ip}}{M/2}, \quad (19)$$

where  $W_{ip}$  is taken from either Eq. (13) for write-once materials or Eq. (14) for rewritable materials. The value  $M/2$  is used because it is assumed that half of the holograms will be multiplexed by shifts in the plane of the reference and signal beams, whereas the other half of the holograms are to be multiplexed through an out-of-plane, or radial, shift.

Finally, the storage density can be calculated when we combine Eqs. (6), (17), (19), and (15). The final density is then

$$D = \frac{N_p}{\max(\delta_M, \delta_s)(W_{op}/2)}. \quad (20)$$

Simply put, this is the number of bits per holographic data page divided by the effective area for each hologram. The effective area of each hologram is half of the width in the radial direction multiplied by the in-track shift that is required, the maximum required by either selectivity or the  $M/\#$  limit. Half of the radial width is used because that is the shift required to cause a reconstructed hologram to rotate completely off the detector and will allow twice as many holograms to be recorded in the same area, compensating for the  $M/2$  used in Eq. (19).

Although use of Eq. (20) to compute the surface storage density appears simple, embedded in it are several parameters that may need to be optimized depending on the particular situation to be modeled. Typically these are the reference beam angle  $\theta_r$ , the signal beam angle  $\theta_s$ , the reference beam divergence  $\phi$  and position  $x_r, z_r$ , the pixel size  $b$ , the imaging lens  $f, A$ , and material thickness  $L$ . Other parameters are typically fixed, such as the  $M/\#$  and the index of refraction  $n$ . Also, for a given system the amount of noise will dictate the required diffraction efficiency  $\eta$  needed to obtain an acceptable SNR. While attempting to solve numerically for the parameters that maximize the storage density, we discovered that local extrema exist in the function. Typically, when the number of parameters to be optimized exceeded two, use of gradient-descent approaches to maximize the density function resulted in solutions depending on the initial parameter values. To circumvent this limitation, a genetic algorithm<sup>12</sup> approach was employed for optimizations.

### 3. Comparison with Experimental Results

To confirm the accuracy of the density calculations, experiments were performed with both a photorefractive crystal ( $\text{LiNbO}_3:\text{Fe}$ ) and the write-once material phenanthrenequinone- (PQ-) doped poly-(methyl methacrylate) (PMMA).<sup>6</sup> The experimental system used is shown in Fig. 5. This system is similar to the system used in Ref. 13. The imaging lenses were Nikon  $F/1.4$  camera lenses with a 50-mm focal length and were experimentally determined to image 590,000 45- $\mu\text{m}$  pixels. The last two lenses and filter were used to block light scattered from the material and optics in front of the material. When the scatter noise is reduced, a lower diffraction efficiency is required to obtain a sufficient signal quality.

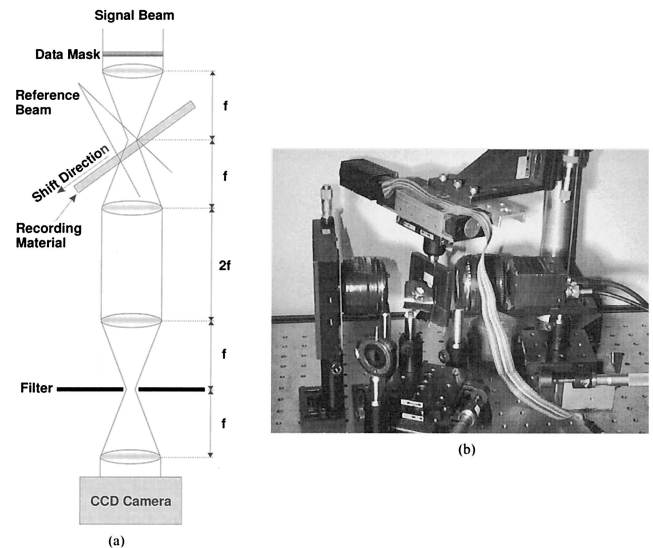


Fig. 5. (a) Holographic data-storage system used for shift multiplexing with PQ-doped PMMA. (b) Photograph of the system used for shift multiplexing with  $\text{LiNbO}_3:\text{Fe}$ , without the additional filtering stage.

A 488-nm laser was used for all experiments. The specifics for each experiment are detailed Subsections 3.A and 3.B.

#### A. Storage Density with $\text{LiNbO}_3:\text{Fe}$

The optical system was configured to have each angle of the signal and reference beams at 35 deg from the normal to the material's surface. A chrome-on-glass mask was used as the data page with a rectangular array of 45- $\mu\text{m}$  square pixels, each randomly set to be either opaque or transparent. The reference beam was created with an  $F/1.1$  lens, giving a divergence angle of  $\phi_r = 48$  deg. Each hologram was recorded at the second null, a shift distance of 7.8  $\mu\text{m}$ , to avoid cross talk. A scan across a track of several recorded holograms is shown in Fig. 6, where the diffraction efficiency of the reconstruction was measured as the

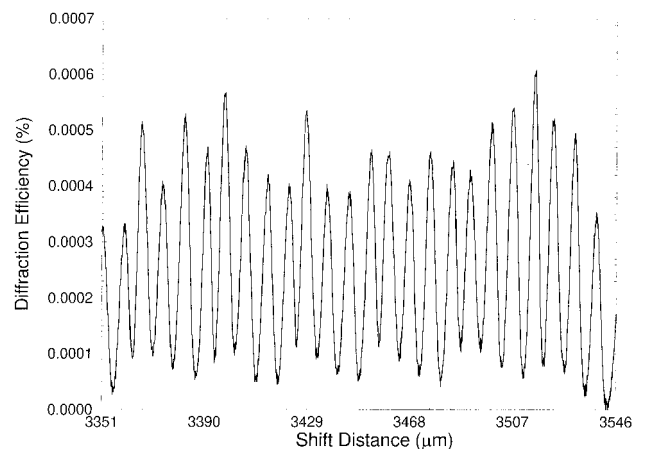


Fig. 6. Shift selectivity of multiple holograms recorded with shift multiplexing in a 1-mm-thick  $\text{LiNbO}_3$  crystal. Each hologram was recorded with a separation of 7.8  $\mu\text{m}$ .

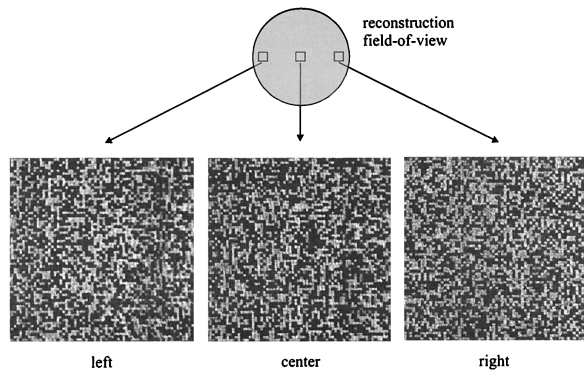


Fig. 7. Left, center, and right sides of a reconstructed hologram for the 100-bits/ $\mu\text{m}^2$  experiment with  $\text{LiNbO}_3$ .

material was translated. Multiple tracks were recorded with a separation of 0.75 mm, enough for the reconstruction to shift off the CCD detector.

At 590,000 pixels/hologram, and a hologram area of  $0.75 \text{ mm} \times 7.8 \mu\text{m}$ , the storage density is 100 bits/ $\mu\text{m}^2$ . The scatter noise integrated over the entire solid angle of the signal beam was measured as  $3.4 \times 10^{-7}$ , relative to the incident reference beam power. The average diffraction efficiency of the recorded holograms was  $4.4 \times 10^{-6}$ . Figure 7 shows the reconstruction of several portions of a single hologram. Because the data mask used was larger than the detector, the detector was translated to capture the reconstruction from several regions to allow a measurement of the reconstruction fidelity. From the distribution of the strengths of the 0 and 1 pixels in the three regions, the SNR was measured to be approximately 4. The method used to determine the SNR is the same as that described in Ref. 13.

We modeled this system using the genetic algorithm, optimizing the density over the focal point position of the reference beam because, for this experiment, the exact position of the reference beam focal point was not measured. The  $M/\#$  was measured to be 1. A slight variation of the calculations described above had to be made to allow the reference beam to come to a focus behind the material, which was the case for the actual experiment. The optimal storage density was found to be 71 bits/ $\mu\text{m}^2$ , whereas the experimentally achieved density was 100 bits/ $\mu\text{m}^2$ . A careful inspection of the calculations showed that, according to Eqs. (5) and (6), only 446,000 pixels are imaged adequately by the  $F/1.4$  lenses. However, these formulas were derived under the typical thin-lens assumption, which is not completely accurate for the seven-element six-group lenses that were being used. Because, according to Eq. (6), the density is proportional to the number of pixels per data page, we can adjust the calculations by scaling to take into consideration the 590,000 pixels/page holograms. This increases the calculated density to 94 bits/ $\mu\text{m}^2$ .

There are several discrepancies between the experimental system and the modeled system. The first lies in the size of the signal beam on the material.

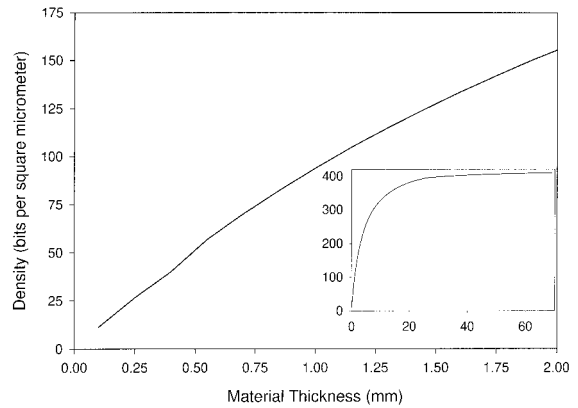


Fig. 8. Storage density in  $\text{LiNbO}_3$  computed as a function of the material thickness with the following parameters:  $\theta_s = 35 \text{ deg}$ ,  $\theta_r = 35 \text{ deg}$ ,  $\phi = 48 \text{ deg}$ ,  $M/\# = 1 \text{ mm}$ ,  $\lambda = 488 \text{ nm}$ ,  $f = 50 \text{ mm}$ ,  $A = 35 \text{ mm}$ ,  $b = 45 \mu\text{m}$ ,  $P = 2$ , and  $\eta = 4.4 \times 10^{-6}$ . The inset shows the same result over an extended range of material thickness in millimeters.

The experimentally measured signal beam was 1.5 mm in diameter on the entrance surface of the material. However, Eqs. (10) predict that the signal beam will occupy 1.76 mm on the entrance surface. The calculated size of the signal beam is 17% larger than what was measured, which is partly due to measurement error. Another cause for the error is again the applicability of the thin-lens assumption. The second difference between the experiment and the calculation is that, in the experiment, the reference beam did not overlap the signal beam on both the entrance and the exit surfaces, but rather complete coverage was obtained only on the entrance surface. However, even with these differences, the calculated density is 94 bits/ $\mu\text{m}^2$  compared with an experimentally achieved value of 100 bits/ $\mu\text{m}^2$ , demonstrating that the calculations are a good predictor of storage densities in rewritable materials.

Figure 8 shows a plot of the calculated storage density as a function of material thickness for this system, where the  $M/\#$  was modeled as increasing linearly with thickness, with a value of one at 1 mm. The storage density increases with thickness, saturating at a value near 410 bits/ $\mu\text{m}^2$ . The density tends to increase with thickness because of an increased  $M/\#$  and better selectivity. However, counteracting these tendencies is the increased area required for the signal and reference beams because of diffraction. There is one caveat to this simulation, however: the assumption that  $M/\#$  increases linearly with thickness. For small deviations in thickness from the thickness at which the  $M/\#$  was measured, this is a valid approximation; however, certainly over the long range plotted in Fig. 8 it is not valid. To maintain a linear increase in  $M/\#$ , the absorption coefficient of the material would have to stay constant, which would effectively decrease the usable thickness of the material because of the lack of beam penetration and correspondingly decrease the measured  $M/\#$  and decrease the hologram selectivity.

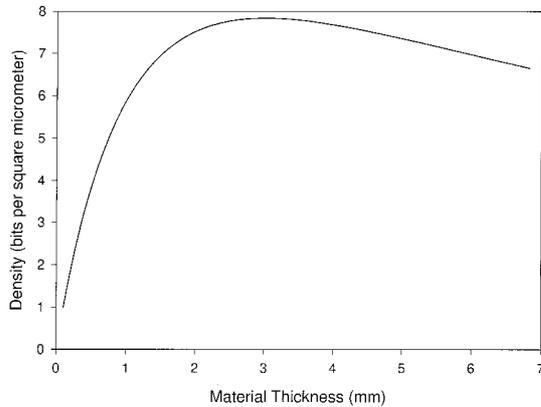


Fig. 9. Simulation of the storage density of PQ-doped PMMA as a function of thickness for the optical system shown in Fig. 5.

#### B. Storage Density with Phenanthrenequinone-Doped Poly(methyl methacrylate)

For this experiment, the recording system was configured for the reference beam to be incident normally onto the material, while we kept the signal beam at a 35-deg angle. A chrome-on-glass data mask was used again, but with square pixels with an edge length of 40  $\mu\text{m}$ . The reference beam came to a focus approximately 2 cm in front of the material, with a divergence angle measured as 8.6 deg. Between hologram exposures the material was shifted normal to the reference in the plane of the recording beams by 50  $\mu\text{m}$ , the distance required to multiplex at the second null for the 3-mm-thick material. The diameter of the signal beam on the material was approximately 1.7 mm, yielding a density of 7 bits/ $\mu\text{m}^2$ . In this case, the holograms were recorded in nonoverlapping tracks. The measured SNR was 3, with an average hologram diffraction efficiency of  $4 \times 10^{-4}$ .

The simulation of this system was made with the actual values for all parameters except for the position of the focal point of the reference beam. Optimization over these two parameters was made because measurement of the exact position relative to the incidence of the signal beam on the material could not be made accurately enough for use in the simulation. For example, when we use the above-quoted focal point distance of 2 cm and optimize the lateral location of the focal point  $x_f$ , the calculations show that it is not possible for the reference beam to overlap the signal beam completely on both surfaces of the material. The simulation was performed for material thicknesses between 100  $\mu\text{m}$  and 4.8 mm, with the  $M/\#$  of the material modeled as a linear function of the thickness, with the measured value of 4.8 at 3 mm. The required diffraction efficiency was  $4 \times 10^{-4}$ , which was obtained experimentally. Figure 9 contains a plot of the results of the simulation. The density computed for a 3-mm-thick material is 7.8 bits/ $\mu\text{m}^2$ , with a focal point position of  $z_f = 2.5$  cm and  $x_f = -1.9$  mm. Such a high value for diffraction efficiency was required because of the high scattering of approximately  $2.8 \times 10^{-4}$  from this material. By

comparison, in the experiment with  $\text{LiNbO}_3:\text{Fe}$  the scatter was measured as only  $3.4 \times 10^{-7}$ , allowing holograms with a diffraction efficiency of only  $10^{-6}$ .

The calculated density is close to the experimentally achieved value, and the optimal focal point position is close to what was measured experimentally. Some factors that cause differences include the exact reference beam positioning as well as the positioning of the signal relative to the material, which both act to decrease the actual storage density achieved. One shortcoming of the simulation causes the predicted values to be somewhat lower than what should be achievable if the exact optical system required could be realized. The shortcoming is the assumption that, for the write-once materials only, the area of the hologram is taken to be the entire area of the reference beam. However, for the location where only the reference beam is incident, and the signal is not, the illumination intensity is half of that where both beams overlap. Therefore the dynamic range of the material is not consumed as quickly as in the areas where both beams overlap, and more holograms should be able to be overlapped than are computed, which would increase the computed storage density slightly.

#### 4. Conclusion

As a final exercise, we applied the storage density model to calculating the density obtainable with a fixed optical system as a function of the  $M/\#$ . One application for holographic data is the read-only disk, in which it would be desirable to have a 12-cm-diameter disk used for storing approximately 100 Gbytes of information, or a density of approximately 85 bits/ $\mu\text{m}^2$ . One obstacle to the realization of such a system is the availability of an adequate holographic recording material. Therefore it is helpful to know the properties required of a recording material before a high-density holographic disk can be successfully implemented. To model such a system, the material's index of refraction was fixed at 1.5, a typical value for polymer materials. We simulated the system assuming lenses with a focal length of 13 mm and a diameter of 11.8 mm. The density was then maximized by the parameters of pixel size  $b$ , focal point position  $x_f$  and  $z_f$ , signal beam angle  $\theta_s$ , reference beam angle  $\theta_r$ , and divergence angle  $\phi_r$ . For practical reasons, the pixel size was limited to a minimum of 1  $\mu\text{m}$ , and the reference beam divergence angle was limited to a maximum of 90 deg. Furthermore, the required diffraction efficiency of the holograms was  $4 \times 10^{-4}$ , separated by two null spacings.

Figure 10 shows the results of six simulation runs with various material thicknesses and two different wavelengths. It is interesting to note that, for a given  $M/\#$  and wavelength, a thinner material will yield a higher storage density until the  $M/\#$  gets large enough that selectivity becomes the primary constraint. A comparison between the density curves for a system using 400-nm light shows that a 0.5-mm-thick material will yield the highest density until the  $M/\#$  reaches approximately 20, at which

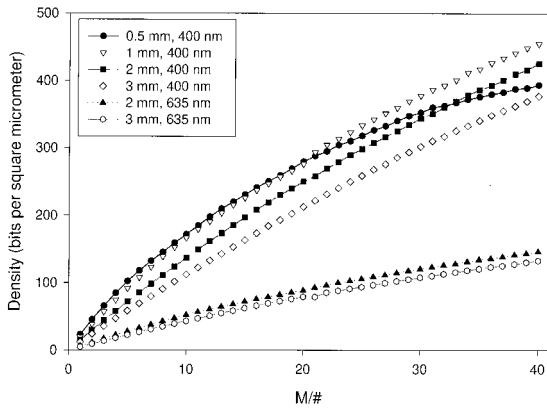


Fig. 10. Theoretical storage density for various wavelengths and material thicknesses as a function of increasing  $M/\#$ .

point a 1-mm-thick material, with its better selectivity, will allow higher storage densities. An important result is the revelation that a large thickness is not an absolute requirement to achieve high densities because a 0.5-mm-thick material should be able to achieve storage densities well in excess of  $100 \text{ bits}/\mu\text{m}^2$ . For many materials the  $M/\#$  is approximately linear with thickness about a small range, and if a comparison is made between the storage density of a thicker material with a thinner material with a correspondingly reduced  $M/\#$ , the thicker material will have a higher potential storage density. For example, if a recording material were 3 mm thick with  $M/20$ , then the system that uses 400-nm light could be expected to achieve a storage density of approximately  $200 \text{ bits}/\mu\text{m}^2$ . However, if the same material were used to make a 2-mm-thick recording media, then it would have approximately  $M/13$  and the corresponding density would be approximately  $175 \text{ bits}/\mu\text{m}^2$ . The other important result of these simulations is the dramatic density improvement that results from the use of shorter wavelengths. Once the  $M/\#$  exceeds a value of 10, there is at least a factor of 2 increase in density even when we are comparing a 2-mm- to a 3-mm-thick material. The performance gained for thinner materials is even greater because the divergence of the signal beam is larger for smaller wavelengths. For large  $M/\#$ 's, the density closely scales with the familiar  $1/\lambda^3$ . This is an expected result because for large  $M/\#$ 's the dynamic range is not an issue, and the density is limited by geometric constraints.

We have presented a straightforward method for computing the storage density of shift-multiplexed holographic memories that addresses the issues of geometry as well as the  $M/\#$ . Furthermore, crosstalk noise can be accounted for in the calculations

when it is required that shifts between holograms be a predetermined number of null spacings of the hologram selectivity function. Optimizations of the derived formulas, with the assistance of a genetic algorithm, have been shown to agree reasonably well with data-storage experiments conducted with both photorefractive and write-once materials. As a result, the analysis presented here can be of assistance in the design and optimization of future holographic memory systems whose performance is limited by the capabilities of the recording material. Furthermore, the simulations can provide an indication of the requirements for a recording material to achieve a desired storage density.

This research was sponsored by the U.S. Air Force Office of Scientific Research and the TRW Foundation. G. J. Steckman acknowledges support from an Intel Foundation Fellowship.

## References

1. P. J. van Heerden, "Theory of information storage in solids," *Appl. Opt.* **2**, 393–400 (1963).
2. K. Buse, A. Adibi, and D. Psaltis, "Non-volatile holographic storage in doubly doped lithium niobate crystals," *Nature* **393**, 665–668 (1998).
3. D. Lande, S. S. Orlov, A. Akella, L. Hesselink, and R. R. Neurgaonkar, "Digital holographic storage system incorporating optical fixing," *Opt. Lett.* **22**, 1722–1724 (1997).
4. H. Guenther, R. Macfarlane, Y. Furukawa, K. Kitamura, and R. Neurgaonkar, "Two-color holography in reduced near-stoichiometric lithium niobate," *Appl. Opt.* **37**, 7611–7623 (1998).
5. L. Dhar, K. Curtis, M. Tackitt, M. Schilling, S. Campbell, W. Wilson, and A. Hill, "Holographic storage of multiple high-capacity digital data pages in thick photopolymer systems," *Opt. Lett.* **23**, 1710–1712 (1998).
6. G. J. Steckman, I. Solomatine, G. Zhou, and D. Psaltis, "Characterization of phenanthrenequinone-doped poly(methyl methacrylate) for holographic memory," *Opt. Lett.* **23**, 1310–1312 (1998).
7. D. A. Waldman, H.-Y. S. Li, and M. G. Horner, "Volume shrinkage in slant fringe gratings of a cationic ring-opening holographic recording material," *J. Imaging Sci. Technol.* **41**, 497–514 (1997).
8. G. Barbastathis, M. Levene, and D. Psaltis, "Shift multiplexing with spherical reference waves," *Appl. Opt.* **35**, 2403–2417 (1996).
9. H.-Y. S. Li and D. Psaltis, "Three-dimensional holographic disks," *Appl. Opt.* **33**, 3764–3774 (1994).
10. J. R. Wullert II and Y. Lu, "Limits of the capacity and density of holographic storage," *Appl. Opt.* **33**, 2192–2196 (1994).
11. F. H. Mok, G. W. Burr, and D. Psaltis, "System metric for holographic memory systems," *Opt. Lett.* **21**, 896–898 (1996).
12. D. Coley, *An Introduction to Genetic Algorithms for Scientists and Engineers* (World Scientific, London, 1999).
13. A. Pu and D. Psaltis, "High-density recording in photopolymer-based holographic three-dimensional disks," *Appl. Opt.* **35**, 2389–2398 (1996).